*American Mineralogist, Volume 76, pages 42–48, 1991*

# The effects of Al and vacancies on Li substitution in iron staurolite: A synthesis approach

**Barbara Dutrow***
Institut für Mineralogie, Ruhr Universität, D-4630 Bochum, Germany

## Abstract

Synthesis of a variety of single phase iron lithium staurolite samples (at 720 °C, 30 kbar, $f_{O_2}$ = IW) demonstrates that a saturation level of Li is attained in iron staurolite at ~1.5 Li ions per 48 O via the substitution $^{[4]}Li^{+} + 0.33^{[6]}Al^{3+} = {}^{[4]}Fe^{2+} + 0.33^{[6]}\square$. Synthesis experiments designed to investigate the substitution $Li^{+} + Al^{3+} = 2Fe^{2+}$ produced substantial amounts of corundum which implies that this substitution is not the primary mechanism responsible for Li incorporation into staurolite. Because Al is charge coupled with Li, the Li maximum appears to be dependent on the vacancies available for the concomitant Al incorporation. Synthesis of two compositional iron staurolite series with differing amounts of Si, 7.5 and 8 pfu, but similar vacancy contents, produced similar results. Utilizing several simplifying assumptions, Al(3A, 3B) octahedra appear to be fully occupied at Li = ~1.5 pfu; site occupancy and bond strengths prohibit additional Li substitution. At more Li-Al-rich compositions, Al and Li phases form in addition to staurolite producing the assemblage staurolite + corundum + $\alpha$-spodumene, at these *P-T-X* conditions.

Lattice parameters of the synthetic staurolite vary linearly as a function of Fe-Li composition with the most pronounced variation occurring in the *b* dimension. The 060 diffraction peak also shifts systematically as a function of Li substitution. Its position potentially provides a method to estimate Li contents in natural Fe-rich staurolite after compensating for shifts caused by substitution of other ions.

The maximum Li contents in staurolite will displace the upper thermal stability of the equilibrium of st + qtz = alm + sill + fluid approximately 40 °C. The displacement to higher *T* will, however, be moderated in most natural settings because of the nonideal Fe-Li mixing in staurolite, the partitioning of Li into coexisting phyllosilicates and the addition of other components.

## Introduction

Staurolite, $(Fe,Mg,Li,Zn)_{4.0-3.3}(Al,Fe^{3+})_{18}(Si,Al)_8O_{48}H_{2.8-4.2}$, a common mineral of predominantly amphibolite grade metapelitic schists, has been considered an enigmatic mineral (e.g., Donnay and Donnay, 1983; Pigage and Greenwood, 1982; Ungaretti et al., 1987). This arises, in part, from inconsistencies encountered when comparing temperatures determined from experimental phase equilibrium studies of staurolite (Richardson, 1968; Ganguly, 1972; Rao and Johannes, 1979) to natural occurrences where temperatures have been estimated by other geothermometric methods. These discrepancies may be partially attributable to staurolite's chemical diversity combined with difficulty in adequately accounting for its structural and chemical complexity.

Numerous workers have shown staurolite to have extremely variable chemistry (see reviews by Holdaway et al., 1986a, 1986b; Donnay and Donnay, 1983 and references therein). This chemical diversity stems not only from numerous homovalent substitutions such as the common $MgFe_{-1}$ exchange component, but also from several heterovalent exchanges. These permit changes in the dominant cations, variations in the H content and allow substantial amounts of monovalent Li to be incorporated into the structure.

Recently Li has been demonstrated to be a significant substituent in staurolite from metapelites (Dutrow et al., 1986). Li was found to be present in all of 31 analyzed metapelitic staurolite samples, with 70% containing greater than 0.1 ion per 48 O. Under special circumstances substantial amounts of Li concentrate in staurolite: greater than 1.0 ion per 48 O, equivalent to 25% occupancy of the tetrahedral Fe sites. This high concentration, however, does not represent the upper limit of Li incorporation into the staurolite structure because there was no coexisting Li-saturating phase. Partitioning studies indicate that staurolite incorporates Li greater than other coexisting pelitic phases (st > crd > bio > mus ≫ grt ≫ tur; Dutrow et al., 1986; mineral abbreviations after Kretz,

* Present address: Department of Geology, University of Iowa, Iowa City, Iowa 52242, U.S.A.

0003–004X/91/0102–0042$02.00

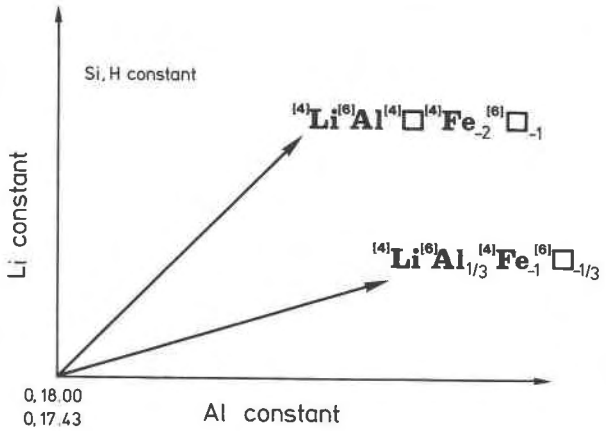


Fig. 1. Substitution schemes for synthetic iron lithium staurolite described by exchange vectors. Coordinates in the lower left represent the initial Li and Al concentration, respectively, in ions per 48 O, for starting compositions A and B. Si and H remain constant along each vector. See text for details.

**Table 1.** Lattice parameters for synthetic iron lithium staurolite

| | *a* (Å) | *b* (Å) | *c* (Å) | *V* (Å³) minerals |
|---|---|---|---|---|
| Composition A*: | $Fe_4Al_{18}Si_{7.5}O_{48}H_4$ | | | |
| $Fe_4Li_0$** | 7.869(3)† | 16.641(4) | 5.660(1) | 741.2 st† |
| $Fe_{3.75}Li_{0.25}$ | 7.866(1) | 16.630(1) | 5.658(1) | 740.2 st |
| $Fe_{3.5}Li_{0.5}$ | 7.865(2) | 16.620(1) | 5.657(1) | 739.5 st |
| $Fe_{3.25}Li_{0.75}$ | 7.867(2) | 16.602(2) | 5.657(2) | 738.9 st |
| $Fe_3Li_1$ | 7.867(2) | 16.600(5) | 5.657(2) | 738.6 st |
| $Fe_{2.75}Li_{1.25}$ | 7.870(1) | 16.583(3) | 5.652(2) | 737.8 st, tr. crn‡ |
| $Fe_{2.5}Li_{1.5}$ | 7.869(2) | 16.571(1) | 5.655(5) | 736.5 st, tr. crn |
| $Fe_{2.25}Li_{1.75}$ | 7.874(2) | 16.577(2) | 5.651(2) | 737.6 st, spd, crn |
| Composition B: | $Fe_4Al_{17.49}Si_8O_{48}H_{\sim 4}$ | | | |
| $Fe_{3.5}Li_{0.5}$ | 7.865(1) | 16.606(3) | 5.654(1) | 738.5 st |
| $Fe_3Li_1$ | 7.867(1) | 16.595(3) | 5.654(1) | 738.2 st |
| $Fe_{2.5}Li_{1.5}$ | 7.872(1) | 16.580(4) | 5.650(1) | 737.5 st, tr. crn |
| Substitution 1: | | | | |
| $Fe_3Li_1Al_{19}$ | 7.869(2) | 16.579(3) | 5.651(1) | 737.3 st, crn, +? |

*Note:* $T = 720$ °C, $P = 30$ kbar, $f_{O_2}$ = IW; all $\beta \sim 90°$.
* Starting composition for substitution 2: $Li^+ + 0.33\,Al^{3+} = Fe^{2+} + 0.33\square$.
** Fe-Li = ions per 48 O, 0.33 Al coupled with each Li.
† Standard errors given in ( ) refer to last decimal place.
‡ tr. = trace, mineral abbreviations after Kretz (1983).

1983). Because of preferential Li partitioning the *P-T* stability regime for staurolite will be modified.

This study investigates the substitution of Li in iron staurolite through a series of synthesis experiments. These experiments provide information on the saturation limit of Li in the structure, factors controlling Li incorporation, variation in unit cell dimensions as a function of Li content, and estimation of Li contents in natural samples. These data also allow an estimate of the maximum effect of Li upon staurolite stability.

## Experimental procedure

### Choice of compositions

Two substitutions have been proposed for the incorporation of Li into staurolite. Their exchange vectors are shown in Figure 1. Proposed substitution 1, $Li^+ + Al^{3+} = 2Fe^{2+}$, is the dominant mechanism responsible for Li entering mica and amphibole (Černý and Burt, 1984) and has also been suggested to account for Li in staurolite (Grew and Sandiford, 1984; Ward, 1984). However, based on a weighted least squares regression of natural staurolite samples, a more accurate substitution scheme was derived: substitution 2, $^{[4]}Li^+ + 0.33^{[6]}Al^{3+} = {}^{[4]}Fe^{2+} + 0.33^{[6]}\square$ (Dutrow et al., 1986). Consequently, compositions for the majority of staurolite samples synthesized in this study were prepared in accordance with substitution 2.

For substitution 2, two starting compositions were chosen; (A) $Fe_4Al_{18}Si_{7.5}O_{48}H_{\sim 4}$ (used by Ganguly, 1972; Griffen, 1981; cf. Richardson, 1968) and (B) $Fe_4Al_{17.43}Si_8O_{48}H_{\sim 4}$. Al and Si values for the latter end-member were deduced by subtracting Li and the corresponding amount of Al according to substitution 2, from natural samples analyzed by Holdaway et al. (1986a). Although natural samples contain Si contents of <8.0 pfu, 8.0 Si were required to maintain charge balance with the calculated amount of Al. In addition, charge balance constraints require $H_{\sim 4}$, consistent with H contents characteristic of high *P* staurolite (Holdaway et al., 1986a). Staurolite compositions defined by substitution 1 were also synthesized to ascertain the plausibility of this substitution.

### Experimental methods

Synthetic lithian staurolite samples were prepared from crystalline mixes of reagent grade iron metal, $Fe_2O_3$, $Al_2O_3$, $SiO_2 \cdot nH_2O$ and synthetic $Li_2SiO_3$ combined in stoichiometric proportions according to the above substitutions at intervals of 0.25 Li ions (Table 1). A double capsule technique was utilized as required by the presence of Fe. Approximately 40 mg of the oxide mixture was packed into an inner AgPd capsule containing a small amount of $H_2O$, sealed, placed within a larger volume Au capsule and surrounded by iron metal powder with sufficient $H_2O$ to produce $Fe_{1-x}O$, wustite (Bohlen and Liotta, 1986). This defined $f_{O_2}$ conditions equivalent to the iron-wustite buffer (IW; Eugster and Wones, 1962) and assured that most Fe was ferrous.

Synthesis experiments were performed in the piston-cylinder apparatus at 720 °C and 30 kbar (±1%). *P* and *T* were automatically regulated. A second series was synthesized at 20 kbar. The outer cylinder of the furnace assembly consisted of NaCl and steel to accommodate the large sample volume and has been described by Massonne and Schreyer (1986). Modifications to their Type I consisted of placing a fired pyrophyllite sheath around and above the Au capsule which served to isolate the chromel-alumel thermocouple from the top of the capsule by 0.5 mm. Because of the length of the inner capsule (~8 mm), longitudinal sample gradients in the inner capsule were ~15 °C (Leistner, 1979). A symmetric *T* distribution was assumed and the capsule center was placed at $T_{max}$. Thermocouple emf readings were corrected ac-

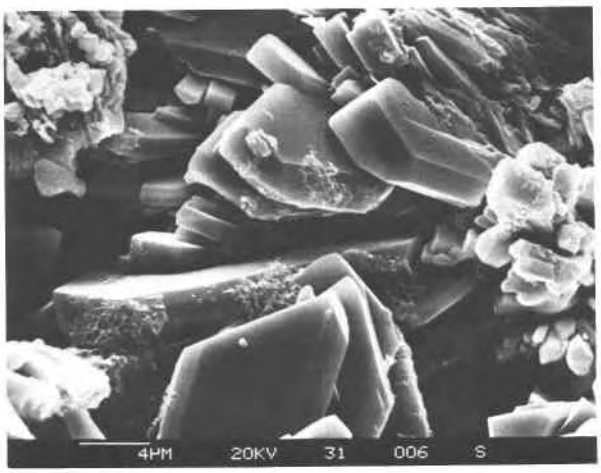


Fig. 2. Secondary electron image of synthetic iron lithium staurolite $Fe_3Li_1Al_{18.33}Si_{7.5}O_{48}H_4$. Bar scale is 4 $\mu$m.

cording to Getting and Kennedy (1970). Experiment durations of 1 d were chosen although Griffen (1981) used a much shorter synthesis time (20 min) with no apparent change in the results.

Experimental products were examined optically, with the scanning electron microscope (SEM), and by X-ray powder diffraction (XRD). Where individual crystals were observed optically, they were well formed, displayed a bladed habit, and were typically very small (1–8 $\mu$m, Fig. 2) thereby precluding most optical and electron beam measurements. The buffer was examined optically and occasionally by X-ray to assure its capacity to buffer $f_{O_2}$ had been maintained. An initial indication of the maintenance of buffering capabilities was provided upon opening the capsules. When all phases were present, the buffer was extremely hard and capsules were difficult to open.

Chemical changes of the staurolite were monitored by unit-cell parameters. Approximately 8 mg of the synthetic material was ground under acetone and mounted for obtaining unit-cell dimensions.

### Lattice parameters

Unit-cell parameters were calculated from X-ray diffraction patterns of up to 50 peaks in the $2\theta$ range 8–80°, obtained with an automated Siemens type D500 diffractometer using graphite monochromatized Cu$K\alpha$ radiation at 45 kV and 25 mA and a goniometer step scan rate of 0.01°/4 s. Synthetic fluorphlogopite (National Bureau of Standards, standard reference material 675) served as the internal standard because it provides calibration at low as well as high $2\theta$ values, with a minimum of peak overlap.

Reflections were indexed according to Borg and Smith (1969). Although the monoclinic character of these synthetic staurolite samples could not be definitely demonstrated (as crystal size was too small to permit single crystal measurements), by analogy with natural staurolite they were refined assuming monoclinic symmetry with $\beta \sim 90$. The $hkl$ and $h0l$ peaks were assigned a double index (e.g., $hkl$ and $\bar{h}kl$) to avoid biasing the $\beta$ angle and to allow comparison with parameters of other synthetic staurolite samples (Griffen, 1981). Lattice parameters were calculated using the refinement program of Appleman and Evans (1973) and are listed in Table 1 with standard errors.

## Results

Single phase, well crystallized staurolite, which varied as a function of the substitution $Li^+ + 0.33\ Al^{3+} = Fe^{2+} + 0.33\square$, inclusive of $Fe_3Li_1Al_{18.33}Si_{7.5}O_{48}H_{\sim 4}$, was produced in experiments beginning with composition A. Traces of corundum (unreacted Al?) appeared in experiments at $Fe_{2.75}Li_{1.25}$ and $Fe_{2.5}Li_{1.5}$. Unit-cell dimensions of these staurolite samples did not appear to be noticeably affected by the presence of corundum as the calculated values retained the trend established by the higher iron staurolite data (Fig. 3). At Li contents equivalent to 1.75 Li pfu, $\alpha$-spodumene appeared in addition to staurolite and corundum, suggesting the saturation limit of Li, Al, or both in the staurolite structure had been exceeded for these $P$-$T$-$X$ conditions. With continued substitution of Li and Al, modal amounts of spodumene and corundum increased proportionately. Staurolite was the only Fe-bearing phase detected in any starting mixture that contained Fe. At compositions equivalent to the Li-Al end-member staurolite, the only phases detected were $\alpha$-spodumene and corundum.

Because traces of corundum without spodumene appeared in several experiments (Table 1), staurolite samples with lower initial Al, composition B ($Fe_4Al_{17.43}Si_8O_{48}H_4$), were synthesized. Synthesis along this compositional series also produced single phase staurolite, until traces of corundum appeared at $Fe_{2.5}Li_{1.5}$. Spodumene and substantial amounts of corundum formed at $Fe_{2.25}Li_{1.75}$ (Table 1). The lower initial Al contents did not appear to alter conclusions based on the higher Al series (see below).

Synthetic mixtures corresponding to the $Li^+ + Al^{3+} = 2Fe^{2+}$ substitution (i.e., $Fe_2Li_1Al_{19}Si_{7.5}O_{48}H_4$) resulted in significant modal amounts of corundum with only minor replacement of Fe by Li-Al. This suggests that substitution 2 is the more probable in iron staurolite.

## Crystal chemistry

Results suggest that the limit of Li in staurolite is controlled by crystal chemistry. As Al, or another trivalent cation of appropriate size, must increase proportionally with Li to maintain electrical neutrality, occupancy of Al(3A, 3B) octahedra may predispose the amount of Li that can be incorporated. [Site names after Smith (1968).] The staurolite structure consists of layers of essentially kyanite (structurally and compositionally) alternating with iron aluminum hydroxide monolayers parallel to $b$ (Náray-Szabó, 1929; Hurst et al., 1956; Smith, 1968; Griffen and Ribbe, 1973; Ribbe, 1982; see also Holdaway et al., 1986a for crystal structure diagrams). Assuming that the kyanite layer is fixed in composition and essentially pure $Al_2SiO_5$ (Smith, 1968; Ståhl et al., 1988), most of the

chemical diversity occurs within the iron aluminum hydroxide monolayer (Griffen, 1981) which is characterized by numerous partially occupied sites and sites which permit extensive and diverse substitution. Bond valence calculations suggest that with the exception of O(5), each O atom in the FeOH layer must be bonded to at least one cation in the layer as well as to those in the kyanite layer (see Holdaway et al., 1986a). In addition, each O atom must have at least one adjacent cation vacancy (Holdaway et al., 1986a). No positional disorder was observed at the Al(3A, 3B) sites by Smith (1968), suggesting that for each Al(3A) octahedron occupied by Al, the adjacent P(1) H positions (Takéuchi et al., 1972) are vacant, or conversely, if P(1A) is occupied, Al will be absent from the octahedron (i.e., H and Al are not expected to occupy one octahedron simultaneously). In addition, bond strengths at O(1A) and O(1B) are not sufficient to support the attachment of Al, H, and Fe or Li simultaneously (Holdaway et al., 1986a). Assuming that Li enters the $^{[4]}$Fe site because of the similarity in size of tetrahedrally coordinated Li and Fe (Shannon, 1976; see also Mössbauer data of Dyar et al., 1991), Al must enter one of the Al(3A, 3B) sites simultaneously, with H being present in the alternate Al(3A, 3B) site. Li is not expected to enter the octahedral site because of the large relative differences between octahedral Li (0.76) and Al (0.535) (see also Holdaway et al., 1986a for cation correlations).

Utilizing the simplifying assumptions of a fully ordered staurolite (Hanisch, 1966; cf. Fitzpatrick, 1976; Wenk, 1980; Lefebvre, 1982; Ungaretti et al., 1987), a starting composition of $Fe_4Al_{18}Si_{7.5}O_{48}H_4$, all Fe as $Fe^{2+}$, and the validity of the substitution $Li^+ + 0.33Al^{3+} = Fe^{2+} + 0.33\square$, at $Fe_{2.49}Li_{1.51}$ the Al(3A) octahedra will be fully occupied by Al and Al(3B) will have a full compliment of H [at P(1) sites]. At greater Li and Al contents, Li can be incorporated into the $^{[4]}$Fe site, due to the 1-1 exchange in the occupancy of the $^{[4]}$Fe site, but Al cannot. Consequently, corundum is produced. This is the composition at which occupancy and bond strengths prohibit further Al incorporation and consequently the composition at which staurolite is saturated with Li. At greater Li contents, a Li-saturating phase forms, $\alpha$-spodumene at these *P-T-X* conditions, in addition to corundum. Different bulk compositions would produce alternate saturating phases, e.g., lithium mica, sillimanite, holmquistite, etc. The staurolite reported to coexist with amblygonite [a Li-saturating phase, $LiAl(PO_4)F$; von Knorring et al., 1979] should have the maximum Li content attainable in the staurolite structure. Unfortunately, attempts to locate this staurolite were unsuccessful.

Composition B ($Fe_4Al_{17.43}Si_8O_{48}H_{\sim 4}$) has lower initial Al but produced results comparable to those of composition A in terms of Li saturation limit as well as unit-cell dimensions (Table 1). This is most likely attributable to the comparable numbers of vacancies (0.5 and 0.57, respectively) available for Al incorporation. However in composition A, the $^{[4]}$Si site has less than a full complement of 8 Si pfu and presumably contains minor Al, whereas in B, Al was decreased and Si increased.

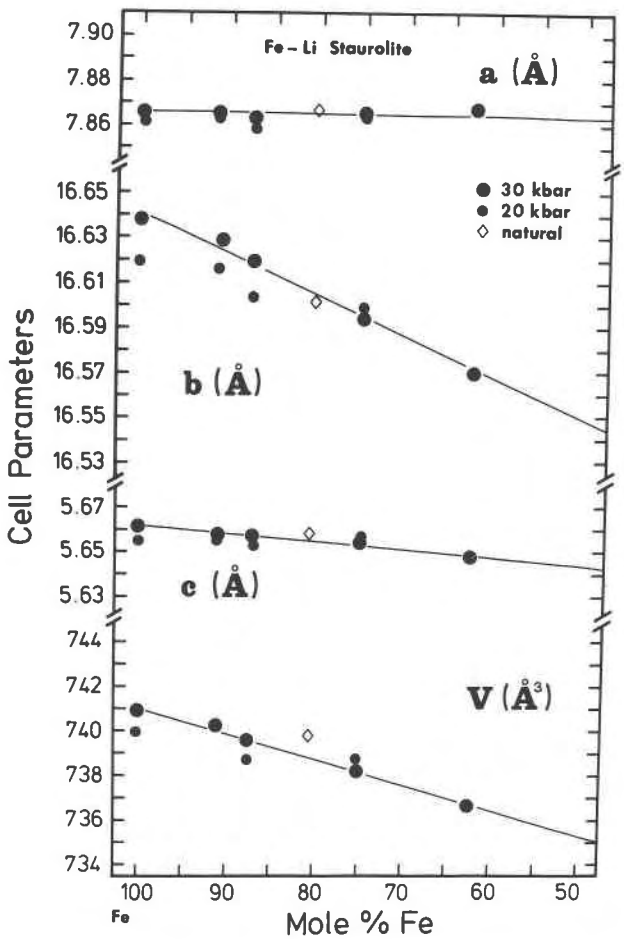


Fig. 3. Variation in unit-cell parameters as a function of Fe-Li composition for substitution 2: $Li^+ + 0.33Al^{3+} = Fe^{2+} + 0.33\square$; starting composition A. Dots represent parameters of synthetic staurolite; diamond, a natural iron lithium staurolite, Truchas Mountains, New Mexico. Errors are listed in Table 1 and approximately given by the size of the symbol.

These results suggest that Li can only enter the staurolite structure when sufficient vacancies exist to accommodate the concomitant incorporation of Al, or another appropriately sized and charged cation. When the Al octahedra are fully occupied, Li can no longer be incorporated because of charge balance constraints. Consequently, Li incorporation depends directly on the vacancy content in addition to Li availability. The limit of Li in staurolite noted here could be enhanced if Al(3A, 3B) octahedral vacancies were increased, H contents were decreased, U-sites were filled, and/or octahedral $Fe^{3+}$ were present. *P-T-X* conditions may indirectly control Li incorporation by dictating the equilibrium H values in staurolite which change as a function of *P, T* and the coexisting assemblage. Many simplifying assumptions have been utilized in order to identify the controlling crystallochemical factors of Li incorporation into staurolite. With more complete structural refinements of staurolite (Hawthorne, in preparation), the validity of the

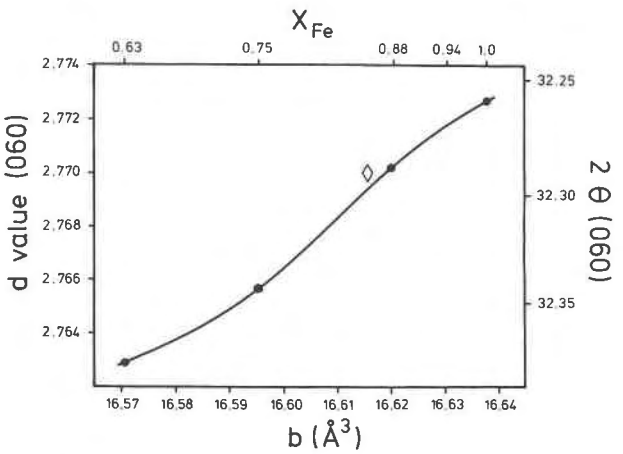


Fig. 4. Position of the 060 diffraction peak for iron lithium staurolite as a function of Li incorporation: substitution 2, composition A. The d value provides a method of estimating Li contents for natural Fe-Li-rich staurolite. Diamond, as in Figure 3.

assumptions of cation location and ordering can be evaluated.

Mössbauer studies completed on several of these staurolite samples indicate that 3–6% of the total Fe is $Fe^{3+}$ (Dyar et al., 1991). Although the location of the $Fe^{3+}$ is not yet resolved, Dyar et al. suggest it is in tetrahedral coordination (Fe or Si site). If $Fe^{3+}$ is in tetrahedral coordination, it would increase the amount of Li that could enter the structure by providing an alternate charge couple. However, $Fe^{3+}$ in octahedral coordination would reduce the amount of Al that could be incorporated thereby lowering the saturation level of Li unless $Fe^{3+}$ acted as the charge coupler. Mössbauer studies do support the substitution of Li in the $^{[4]}$Fe site because of concomitant and proportional reduction in the intensity of $^{[4]}$Fe doublets (occupancy) with increased Li substitution.

The significant modal amounts of corundum produced in experiments investigating substitution 1 presumably result from the inability of staurolite to incorporate the increased amount of Al that is coupled with Li. This provides supportive evidence that substitution scheme 2 is the controlling mechanism by which Li is incorporated into most staurolite samples from metapelites. Substitution 1 is, however, potentially feasible for those staurolite samples with lower H contents, increased vacancies in Al(3A, 3B) octahedra, or both.

Ward (1984) has suggested substitution 1 for the staurolite cited in von Knorring et al. (1979) which contains high Al and coexists with corundum and amblygonite. Ward suggested the presence of substantial Li to account for the high Al and low totals of Fe + Mg + Zn obtained from microprobe analysis. However, the chemical data reported would require far too much Li (>4 atoms per 48 O) in the structure to satisfy charge balance constraints. Alternatively, the low total probably reflects a combination of Li incorporation, $Fe^{3+}$, mineral inclusions, analytical errors in Al, the divalent cation determinations, or both. It is also possible that this staurolite contains substantial quantities of other unanalyzed elements (e.g., light elements) to account for the low microprobe total.

Unit-cell parameters for staurolite synthesized along substitution 2 with starting composition A vary linearly with composition (Fig. 3, Table 1), as has been found for other synthetic staurolite (Griffen, 1981; Phillips and Griffen, 1986). The most marked change is observed in the *b* dimension where the FeOH monolayer decreases substantially in size from the substitution of Li and Al for Fe. Griffen (1981) suggested that this large change apparently results from the ability of the FeOH layer to change its size independently of the kyanite layer. When spodumene appears, *b* reverses its trend and increases in size to values slightly greater than that observed for staurolite without spodumene, suggesting that less Li is entering the staurolite structure (Fig. 3). Along the **a** axis, the Al chains are separated by nearly vacant U sites which collapse or expand easily upon ionic substitution (Griffen, 1981). Consequently, the *a* dimension remains similar despite Li-Al substitution. Parallel to *c,* increasing the amount of Li and Al substitution decreases the length of the chains, but the contraction is limited by the required octahedral-tetrahedral fit to nonexpanding-contracting kyanite layers (Griffen, 1981). Consequently, only slight differences in *c* unit-cell dimensions are noted with changing compositions.

Lattice parameters do not vary substantially between compositional suites A and B (Table 1). The principal difference between these two suites is in the Al vs. Si content which occurs primarily in the kyanite layer. The *a* parameters are similar for all compositions (±0.005, standard error 0.003), in contrast to other synthetic staurolite samples where they decrease slightly with increasing substitution for Fe (Griffen, 1981; Phillips and Griffen, 1986). As expected from size considerations of $^{[6]}$Al (0.39) and $^{[4]}$Si (0.26), staurolite of composition A with 0.5 Al entering the $^{[4]}$Si site has a slightly larger *c* dimension than comparable staurolite of composition B with $^{[4]}$Si = 8 pfu. Although the *b* parameter decreases in both series with the addition of Li-Al, $b_A$ has a greater overall decrease than $b_B$ (0.07 vs. 0.06, ±0.004). In all samples, the $\beta$ angle is nearly 90° (0.02).

The effect of $Fe^{3+}$ on the staurolite lattice parameters is poorly understood because of the uncertainty in the location and amount of $Fe^{3+}$ in staurolite. If the $Fe^{3+}$ replaces tetrahedral Al that has substituted for Si in the kyanite layer (Dyar et al., 1991; although this seems unlikely given the difference in ionic radii between $^{[4]}$Si = 0.26 and $^{[4]}Fe^{3+}$ = 0.49 Å), the net effect would be to increase substantially the *c* dimension and to a lesser extent the *a* dimension. However, if $Fe^{3+}$ enters the $^{[4]}$Fe site (see review by Holdaway et al., 1986a; Dyar et al., 1991), *b* should decrease. $Fe^{3+}$ substitution into the $^{[4]}$Al(3A, 3B) site (Holdaway et al., 1986a) would have little effect on the *b* dimension because the ionic radii of $^{[6]}$Al and $^{[6]}Fe^{3+}$ cations are similar. Minor $Fe^{3+}$ substitution into differing sites could explain some of the scatter

in the unit-cell data. The synthetic staurolite reported here is assumed to contain similar amounts of $Fe^{3+}$ at each pressure, because all syntheses were completed under identical conditions.

Staurolite synthesized under lower $P$ conditions (20 kbar; Fig. 3) consistently displays smaller and less regular unit-cell parameters than that synthesized at higher pressures. This feature, also noted by Griffen (1981), has no obvious explanation.

Molar volume data also vary linearly (within error limits) as a function of composition (Fig. 3). This implies that the volume of mixing is close to zero, that there is no significant pressure effect on nonideality, and that Fe and Li are disordered with respect to one another. The nearly ideal behavior of the Li-Fe exchange may explain the overcorrection of $T$ calculated for natural high lithium staurolite using a nonideal mixing model (Holdaway et al., 1988) and suggests that the Fe-Li interaction is more ideal than Fe-Mg exchange in staurolite.

### Application of results to natural staurolite

Unit-cell data of synthetic staurolite may provide a useful and relatively simple method for estimating Li concentrations in natural iron lithium staurolite. This is illustrated by examining the cell dimensions of a natural high iron lithium and low magnesium zinc staurolite from the Truchas Mountains, New Mexico (see Holdaway et al., 1986a for chemistry) relative to the dimensions of the synthetic phases. As shown in Figure 3, the measured Li value for the Truchas staurolite is very near that predicted by unit-cell dimensions of the synthetic phases. Although this staurolite has few metal cations other than Fe-Li, the above techniques can also be applied to other less binary staurolite samples by correcting for the size of additional metal cations, e.g., Mg, Zn, etc. Therefore, lattice parameters may provide an independent technique for estimating Li contents in Fe-rich staurolite when used in conjunction with microprobe analyses.

Alternatively, Li content of an Fe-rich staurolite sample may be estimated by powder diffraction techniques without obtaining complete unit-cell dimensions by the position of the 060 diffraction peak after compensating for additional nonbinary cations. Figure 4 displays the peak position of 060 as a function of Fe-Li composition of the synthetic staurolite, after correction to the internal standard. For comparison, the position of the 060 peak of the Truchas staurolite is plotted at the appropriate Li concentration.

When applying these techniques to natural assemblages, their utility is limited by the multicomponent nature of staurolite. The above suggestions for estimating Li concentrations, without resorting to ion microprobe or wet chemical analyses, have been based on an idealized system. Corrections for the nonbinary components will have to be made. Nonetheless, as more complete data on the location of the various cations in staurolite become available, more accurate corrections can be made to extrapolate data from the multicomponent system to the simple system presented here.

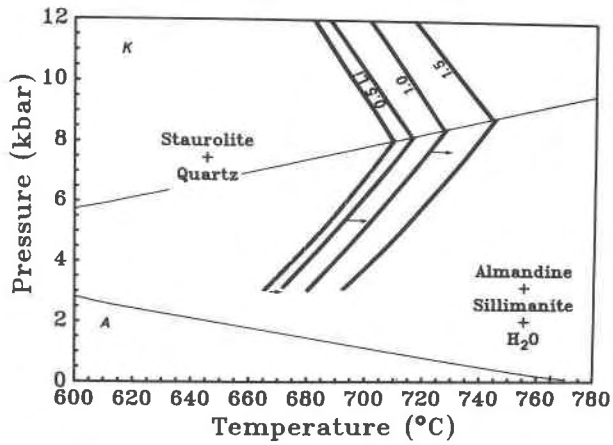


Fig. 5. Displacement of the upper thermal stability of st + qtz = alm + sill + fluid resulting from the incorporation of Li in iron staurolite. Isopleths are calculated at 0.5 Li ion intervals. An ideal activity model for staurolite and thermochemical data derived from experiments of Dutrow and Holdaway (1989) and Dutrow (in preparation) are used. The 0 Li isopleth was experimentally calibrated by Dutrow and Holdaway (1989). Aluminum silicate transition from Holdaway (1971). A = andalusite. K = kyanite.

### Li effect on staurolite stability

One of the more important aspects of Li in staurolite is its effect on staurolite stability. Displacement of the upper thermal stability of the assemblage iron lithium staurolite + quartz, defined by the reaction staurolite + quartz = almandine + sillimanite + fluid, was calculated for various Li concentrations using an ideal solution model for staurolite (Holdaway et al., 1988) and thermochemical data for the above reaction retrieved by the method of Chatterjee (1977) from the results of Dutrow and Holdaway (1989) and Dutrow (in preparation).

An activity model was developed by assuming Al to be coupled with Li; the activity of iron staurolite = $X_{Fe}$ where $X_{Fe}$ was the amount of Fe after Li substitution according to $Li^{+} + 0.33Al^{3+} = Fe^{2+} + 0.33\square$. The actual values of Li were used, although in reality it is difficult to couple ⅓ atom of Al. However, this model permits estimation of the maximum displacement of the staurolite equilibria resulting from the incorporation of Li. Alternatively, one could calculate the shift using Al contents and assume triplets of Li were coupled. This would result in a smaller $T$ shift. If the amount of nonideality were known and included, the temperature shift would also be reduced.

Shown in Figure 5 are isopleths for iron lithium staurolite samples containing 0.5, 1.0, and 1.5 Li pfu. As staurolite strongly partitions Li relative to garnet ($K_d$st/gar = ~50; Dutrow et al., 1986), the upper thermal stability of staurolite in the FLASH system is displaced 40° for the maximum Li contents in staurolite utilizing the above model and assumptions. This results in an increase in the stability field of staurolite with respect to almandine and sillimanite, thus displacing the staurolite-out isograd to higher $T$. This expansion will be mitigated in nature

by the presence and partitioning of Li in coexisting phyllosilicates and by substitutions for Fe in garnet.

Partitioning studies of Li between various coexisting metamorphic minerals reveal that staurolite scavenges Li more than any other phase with which it coexists (garnet, chloritoid, muscovite, biotite, cordierite; Dutrow et al., 1986). This also suggests qualitative displacements of reaction boundaries other than that shown in Figure 5. When stabilized by Li, the initial formation of staurolite should occur at lower $T$ and $P$ with respect to almandine and chlorite or chloritoid. The ultimate effect of Li is the expansion of the entire stability regime for staurolite.

## Acknowledgments

This study was undertaken while the author was an Alexander von Humboldt (AvH) fellow at Ruhr-Universität. My sincere appreciation to W. Schreyer for many discussions and the opportunity to conduct this research in his lab and to the AvH for financially supporting this endeavor. Herr Baller, Herr Anderson, and my Pressenraum coworkers are thanked for providing technical assistance and guidance. Many thanks to A. Fischer for photographic skills, K. Oly for SEM assistance, F. Lorman for drafting, W. Maresch for contributing $Li_2SiO_3$, J. Grambling for the Truchas staurolite, and U. Bednarz and G. Worner for computer drafting. Stimulating discussions with N.J. Chatterjee greatly enriched my research and cultural experience. Initial reviews by D.J. Henry, M.J. Holdaway, and W. Schreyer improved the manuscript. J. Grambling is thanked for his helpful journal review.

## References cited

Appleman, D.E., and Evans, H.T. (1973) Job 9214: Indexing and least-squares refinement of powder diffraction data. U.S. National Technical Information Service, Document PB 216 188.

Bohlen, S., and Liotta, J. (1986) A barometer for garnet amphibolites and garnet granulites. Journal of Petrology, 27, 1025–1034.

Borg, I.Y., and Smith, D.K. (1969) Calculated X-ray powder patterns for silicate minerals. Geological Society of America Memoir, 122.

Černý, P., and Burt, D.M. (1984) Paragenesis, crystallochemical characteristics, and geochemical evolution of micas in granite pegmatities. In Mineralogy Society of America Reviews in Mineralogy, 13, 257–297.

Chatterjee, N.D. (1977) Thermodynamics of dehydration equilibria. In D.G. Fraser, Ed., Thermodynamics in geology, p. 137–160. Reidel, Boston.

Donnay, J.D.H., and Donnay, G. (1983) The staurolite story. Tschermaks Mineralogische und Petrographische Mitteilungen 31, 1–15.

Dutrow, B.L., and Holdaway, M.J. (1989) The upper thermal stability of staurolite + quartz at medium pressure. Journal of Petrology, 30, 229–248.

Dutrow, B.L., Holdaway, M.J., and Hinton, R.W. (1986) Lithium in staurolite and its petrologic significance. Contributions to Mineralogy and Petrology, 94, 496–506.

Dyar, M., Perry, C., Rebbert, C., Dutrow, B., Holdaway, M., and Lang, H. (1991) Mössbauer spectroscopy of synthetic and naturally occurring staurolite. American Mineralogist, 76, 27–41.

Eugster, H., and Wones, D. (1962) Stability relations of ferruginous biotite, annite. Journal of Petrology, 3, 82–125.

Fitzpatrick, J.J. (1976) Studies in the microstructure and crystal chemistry of minerals: I. Burbankite from the Green River Formation, Wyoming II. Electron microscopy of staurolite III. Crystal structure determination of vuagnatite $CaAlSiO_4(OH)$. Ph.D. thesis, University of California–Berkeley, Berkeley, California.

Ganguly, J. (1972) Staurolite stability and related paragenesis. Theory, experiments and applications. Journal of Petrology, 13, 335–365.

Getting, I.C., and Kennedy, G.C. (1970) Effect of pressure on the emf of chromel-alumel and platinum-platinum 10% rhodium thermocouples. Journal of Applied Physics, 41, 4552–4562.

Grew, E.S., and Sandiford, M. (1984) A staurolite-talc assemblage in tourmaline-phlogopite-chlorite schist from northern Victoria Land, Antarctica and its petrogenetic significance. Contributions to Mineralogy and Petrology, 87, 337–350.

Griffen, D.T. (1981) Synthetic Fe/Zn staurolites and the ionic radius of $^{iv}Zn^{2+}$. American Mineralogist, 66, 932–937.

Griffen, D.T., and Ribbe, P.H. (1973) The crystal chemistry of staurolite. American Journal of Science, 273-A, 479–495.

Hanisch, K. (1966) Zur kenntnis der kristallstruktur von staurolith.Neues Jahrbuch für Mineralogie Monatshefte, 362–366.

Holdaway, M.J. (1971) Stability of andalusite and the aluminum silicate phase diagram. American Journal of Science, 271, 97–131.

Holdaway, M.J., Dutrow, B.L., and Shore, P. (1986a) A model for the crystal chemistry of staurolite. American Mineralogist, 71, 1142–1159.

Holdaway, M.J., Dutrow, B.L., Shore, P., and Hinton, R.W. (1986b) H content of staurolite as determined H extraction line and ion microprobe. American Mineralogist, 71, 1135–1141.

Holdaway, M.J., Dutrow, B.L., and Hinton, R.W. (1988) Devonian and Carboniferous metamorphism in west-central Maine: The muscovite-almandine geobarometer and the staurolite problem revisited. American Mineralogist, 75, 20–45.

Hurst, V.J., Donnay, J.D.H., and Donnay, G. (1956) Staurolite twinning. Mineralogical Magazine, 31, 145–165.

Kretz, R. (1983) Symbols for rock-forming minerals. American Mineralogist, 68, 277–279.

Lefebvre, A. (1982) Lattice defects in three structurally related minerals: kyanite, yoderite, and staurolite. Physics and Chemistry of Minerals, 8, 251–256.

Leistner, H. (1979) Temperaturgradienten-Messungen in Piston-Zylinder-Pressen. Fortschritte Mineralogie, 57, 81–82.

Massonne, H.-J., and Schreyer, W. (1986) High-pressure syntheses and X-ray properties of white micas in the system $K_2O$-MgO-$Al_2O$-$SiO_2$-$H_2O$. Neues Jahrbuch für Mineralogie Abhandlung, 153, 177–215.

Náray-Szabó, I. (1929) The structure of staurolite. Zeitschrift für Kristallographie, 71, 103–116.

Phillips, L.V., and Griffen, D.T. (1986) Staurolite-lusakite series. I. Synthetic Fe-Co staurolites. American Mineralogist, 71, 1461–1465.

Pigage, L.C., and Greenwood, H.J. (1982) Internally consistent estimates of pressure and temperature: The staurolite problem. American Journal of Science, 282, 943–969.

Rao, B.B., and Johannes, W. (1979) Further data on the stability of staurolite and quartz and related assemblages. Neues Jahrbuch für Mineralogie Monatshefte, H10, 437–447.

Ribbe, P.H. (1982) Staurolite. In Mineralogy Society of America Reviews in Mineralogy, 5, 171–188.

Richardson, S.W. (1968) Staurolite stability in a part of the system Fe-Al-Si-O-H. Journal of Petrology, 9, 467–488.

Shannon, R.D. (1976) Revised effective ionic radii and systematic studies of interatomic distances in halides and chalcogenides. Acta Crystallographica, A32, 751–767.

Smith, J.V. (1968) The crystal structure of staurolite. American Mineralogist, 53, 1139–1155.

Ståhl, K., Kvick, A., and Smith, J.V. (1988) A neutron diffraction study of hydrogen positions at 13 K, domain model, and chemical composition of staurolite. Journal of Solid State Chemistry, 73, 362–380.

Takéuchi, Y., Aikawa, N., and Yamamato, T. (1972) The hydrogen locations and chemical composition of staurolite. Zeitschrift für Kristallographie, 136, 1–22.

Ungaretti, L., Callegari, A., and Caucia, F. (1987) On the 'Staurolite Enigma'. Terra Cognita, 7, 384.

von Knorring, R., Sahama, T.G., and Siivola, J. (1979) Zincian staurolite from Uganda. Mineralogical Magazine, 43, 446.

Ward, C.M. (1984) Magnesium staurolite and green chromian staurolite from Fiordland, New Zealand. American Mineralogist, 69, 531–540.

Wenk, H.R. (1980) Defects along kyanite-staurolite interfaces. American Mineralogist, 65, 766–769.

Manuscript received March 12, 1990
Manuscript accepted November 17, 1990